RASĀYAN *J. Chem.*
Vol. 19 | No. 3 | 1489-1494 | July-September | 2026
ISSN: 0974-1496 | e-ISSN: 0976-0083 | CODEN: RJCABP
http://www.rasayanjournal.com
http://www.rasayanjournal.co.in

# CORRELATION OF STRUCTURAL, VIBRATIONAL AND ELECTROCHEMICAL PROPERTIES OF $LiNiO_2$ AND $LiNi_{1/3}Co_{1/3}Mn_{1/3}O_2$ CATHODE MATERIALS

**K. V. Babu[1], Y. N. Rao[1], P. Ramakrishna[1], K. S. K. R. C. Sekhar[2], and Ch. Srinivas[3]**

[1]Department of Physics, Centurion University of Technology and Management, Vizianagaram-535 003 AP, India

[2]Department of Physics, Siddhartha Academy of Higher Education, Deemed to be University, Vijayawada-520007, AP, India

[3]Department of Physics, Sasi Institute of Technology & Engineering, Tadepalligudem-534101, AP, India

✉Corresponding author: vijayababu.k@gmail.com

**ABSTRACT**

Layered structure $LiNiO_2$ and $LiNi_{1/3}Co_{1/3}Mn_{1/3}O_2$ were prepared via the sol-gel auto-combustion route at a calcination temperature of 900 ºC. A comprehensive investigation of the structural, vibrational, and electrochemical characteristics of both cathode materials was conducted. The XRD patterns of both the samples were indexed to the α-$NaFeO_2$ layered structure with no detectable impurity phases. The Rietveld refinement was carried out, which confirms the presence of rhombohedral symmetry with a space group of $R\bar{3}m$ . For $LiNi_{1/3}Co_{1/3}Mn_{1/3}O_2$ powders are located at 509.20 and 603.71 $cm^{-1}$. In the electrochemical process, a little reduction in the material's initial capacity is compensated for by a considerable increase in cyclability. These findings support that one of the most appealing cathodes for real-world applications, particularly for high-rate lithium-ion batteries used in electric vehicles.

**Keywords:** Cathode Materials, Lithium Nickel Oxide, XRD, FTIR, Rietveld Refinement, Charge/Discharge Studies.

RASĀYAN *J. Chem.*, Vol. 19, No.3, 2026

## INTRODUCTION

Among energy storage technologies, lithium-ion batteries have emerged as the dominant power source for electric vehicles, owing to their superior energy density, high specific power, and advanced technological maturity. $LiCoO_2$ is the primary cathode material in commercial lithium-ion batteries because of its favorable electrochemical properties and ease of manufacture. Nevertheless, cobalt presents significant limitations as a battery raw material. Its toxicity, environmental hazards, and high market cost are well-documented concerns, and cobalt extraction has raised serious issues regarding labor exploitation. The structural degradation that occurs when $LiCoO_2$ loses more than 0.5 Li limits the usage of $LiCoO_2$ as a cathode material in lithium ion batteries. There is a keen interest in creating substitute, affordable cathode materials due to these restrictions and safety issues. In this context, materials based on mixed Ni, Mn, and Mn have been suggested as potential replacements for $LiCoO_2$ as positive electrode materials. Various layered oxide compositions have subsequently been explored. $LiNiO_2$, $LiNi_xCo_yO_2$, $LiMn_xCo_yO_2$, $LiMn_xNi_yO_2$, $LiNi_xCo_yAl_zO_2$, $LiNi_{1/3}Co_{1/3}Mn_{1/3}O_2$, and other layered compounds sharing hexagonal symmetry derived from the α-$NaFeO_2$ prototype with $R\bar{3}m$ space group have all been investigated. In this, $LiNiO_2$ has been extensively studied in the early decades of lithium-ion batteries.[1,2] However, several fundamental synthesis challenges hindered its commercial viability. Since lithium partially volatilizes at synthesis temperatures and $Ni^{3+}$ is easily reduced to $Ni^{2+}$, the stoichiometric $LiNiO_2$ (Li/Ni ratio of 1:1) is a challenging to synthesize. Additionally, the composition of $LiNi_{1/3}Co_{1/3}Mn_{1/3}O_2$ has an equal number of high-capacity and good rate capability transition metals Ni, Co, and Mn.[3,4] This material has been identified as particularly effective in stabilizing cathode cycling behaviour. The reaction of the mixes of lithium, cobalt, nickel, and manganese nitrates taken in the stoichiometric ratio by the sol-gel auto-combustion process produces $LiNiO_2$ (LNO) and $LiNi_{1/3}Co_{1/3}Mn_{1/3}O_2$ (LNCMO). This synthesis route is


http://doi.org/10.31788/RJC.2026.1939588

widely adopted for Li-ion cathode production due to its operational simplicity, cost efficiency, minimal equipment requirements, and use of commercially accessible starting materials.[5-7] After successful synthesis of these materials, the structural parameters have been investigated through XRD, FTIR and electrochemical properties. The obtained experimental results are compared with well-reported literature.

## EXPERIMENTAL

The $LiNiO_2$ and $LiNi_{1/3}Co_{1/3}Mn_{1/3}O_2$ cathode materials are synthesized by using the sol-gel auto-combustion method. AR grade chemicals such as lithium nitrate ($LiNO_3$), nickel nitrate ($Ni(NO_3)_2.6H_2O$), cobalt nitrate ($Co(NO_3)_2.6H_2O$), manganese nitrate ($Mn(NO_3)_2.4H_2O$) and citric acid ($C_6H_8O_7$) are used for the synthesis process. A 1:1 molar ratio of total metal nitrates to citric acid was employed. The precursors and citric acid were dissolved in an appropriate volume of deionized water, maintaining stoichiometric proportions. Ammonia solution was introduced in controlled amounts to stabilize the pH at 7. The beaker was placed on a magnetic stirrer and agitated continuously to achieve a homogeneous, concentrated solution. Heating was applied gradually until 120 °C, at which point gel formation commenced as the liquid transformed into a viscous medium. Further heating to 200 °C triggered spontaneous auto-ignition of the gel, yielding a porous, ash-like powder that was carefully recovered from the vessel. The as-synthesized powder underwent calcination at 900 °C for 6 hours before structural, vibrational, and electrochemical characterization. Structural identification was performed by X-ray powder diffraction (XRD), vibrational analysis by Fourier transform infrared (FTIR) spectroscopy, and electrochemical behaviour was assessed using a dedicated workstation. XRD data were collected at ambient temperature over a 2θ range of 10–90° employing Cu-Kα radiation (λ = 1.5405 Å). Subsequently, the Rietveld refinement was carried out to examine the phase purity and crystal symmetry quantitatively using the FullProf software package described by a pseudo-Voigt function. The Shimadzu IR-Prestige21 equipment is used to measure Fourier transform infrared (FT-IR) spectra using the transmittance method and potassium bromide (KBr) as an IR window in the wave number range of 400 to 4000 $cm^{-1}$. Galvanostatic cycling characteristics were recorded for CR2032 coin cells using an electrochemical workstation. Phase identification was additionally confirmed via the WinPLOTR graphical interface of FULLPROF.

## RESULTS AND DISCUSSION

### X-ray Diffraction

Figure-1 shows the XRD patterns of $LiNiO_2$ and $LiNi_{1/3}Co_{1/3}Mn_{1/3}O_2$ samples that were produced at 900 ºC for six hours. The produced samples have an a-$NaFeO_2$ layered structure with no extraneous peaks, demonstrating the uniformity and purity of the crystal phase. It is well known that the peak splits of (006)/(102) and (018)/(110), which occur near 37.95° and 64.12° respectively, are signs of layered structures like $LiNiO_2$. The least-square method yielded lattice parameters *a* and c of 2.8577Å and 14.2269 Å, respectively, which are in good agreement with the published works and $LiNiO_2$. The degree of cation mixing in the lattice is best gauged by the intensity ratio of I003/I104 (R). This is frequently used to gauge how much cation mixing has occurred. For a lesser degree of cation mixing, a higher value of R is preferred. Unwanted cation mixing typically occurs when the integrated intensity ratio is less than 1.2. The calculated $I_{003}/I_{104}$ ratio of the $LiNiO_2$ and $LiNi_{1/3}Co_{1/3}Mn_{1/3}O_2$ is 1.4 and 1.3 respectively. The pronounced (003)/(104) intensity contrast and distinct (006, 102) and (108, 110) doublet resolution corroborate the well-defined layered character of both compounds.[8,9] Detailed crystallographic parameters derived from this analysis are compiled in Table-1 alongside reference data from the literature.

### FTIR Spectra

Figure-2 shows the FTIR spectra of $LiNiO_2$ and $LiNi_{1/3}Co_{1/3}Mn_{1/3}O_2$ samples. $LiO_6$ and $MO_6$ octahedra with shared edges alternate in layers to form the crystal structure of the layered oxide $LiNiO_2$. In the instant of $LiNi_{1/3}Co_{1/3}Mn_{1/3}O_2$, the transition metal cations (Ni, Co, and Mn) and lithium ions are situated at Wyckoff sites 3a and 3b, respectively. This site assignment is consistent with the Rietveld refinement data. A two-dimensional structure results from the arrangement of the $Li^+$ and $Co^{3+}/Ni^{2+}/Mn^{4+}$ ions along the rock-salt cubic lattices (111) direction. The two principal absorption bands, with its peak centred at 487.99 and 601.79 $cm^{-1}$, are used to explain the IR absorption bands for $LiNiO_2$. Additionally, the IR bands of $LiNi_{1/3}Co_{1/3}Mn_{1/3}O_2$ powder peaks are situated at 509.20 and 603.71 $cm^{-1}$. The high frequency

bands of the FT-IR absorption spectra of $LiNiO_2$ and $LiNi_{1/3}Co_{1/3}Mn_{1/3}O_2$ located around 600 $cm^{-1,}$ which are attributed to the asymmetric stretching modes of the $MO_6$ group, whereas the other frequency bands around 500 $cm^{-1}$ are allocated to the O-M-O bending vibration.[10-11]

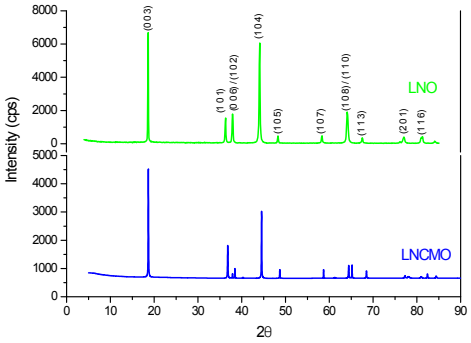


Fig.-1: XRD Pattern of $LiNiO_2$ and $LiNi_{1/3}Co_{1/3}Mn_{1/3}O_2$

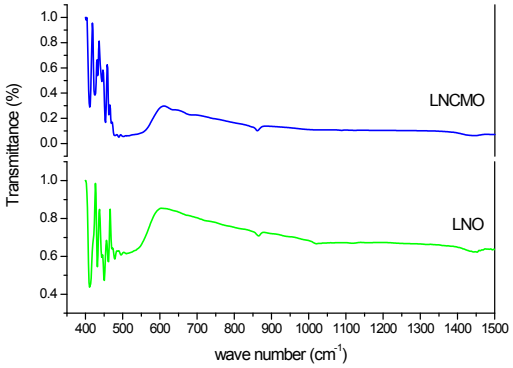


Fig.-2: FTIR Spectra of $LiNiO_2$ and $LiNi_{1/3}Co_{1/3}Mn_{1/3}O_2$

Table-1: Parameters and Reliability Factors obtained by the Rietveld Refinement of $LiNiO_2$ from X-ray Diffraction Pattern

| S.No. | Atom | | *x* | *y* | *z* | *Occ.* | *U* | *Site* | *Sym.* |
|---|---|---|---|---|---|---|---|---|---|
| 1 | O | O1 | 0.00000 | 0.00000 | 0.25277 | 0.065 | 0.956 | 6c | 3m |
| 2 | Li | Li2 | 0.00000 | 0.00000 | 0.00000 | 0.671 | 0.308 | 3b | -3m |
| 3 | Li | Li1 | 0.00000 | 0.00000 | 0.50000 | 0.244 | 0.041 | 3a | -3m |
| 4 | Ni | Ni2 | 0.00000 | 0.00000 | 0.00000 | -0.031 | 0.308 | 3a | -3m |
| 5 | Ni | Ni1 | 0.00000 | 0.00000 | 0.50000 | -0.013 | 0.308 | 3b | -3m |

Table-2: Parameters and Reliability Factors Obtained by the Rietveld Refinement of the of $LiNi_{1/3}Co_{1/3}Mn_{1/3}O_2$ from X-ray Diffraction Pattern

| S.No. | Atom | | *x* | *y* | *z* | *Occ.* | *U* | *Site* | *Sym.* |
|---|---|---|---|---|---|---|---|---|---|
| 1 | O | O1 | 0.00000 | 0.00000 | 0.24360 | 1.000 | -0.100 | 6c | 3m |
| 2 | Co | Co1 | 0.00000 | 0.00000 | 0.50000 | 0.333 | 1.000 | 3b | -3m |
| 3 | Ni | Ni2 | 0.00000 | 0.00000 | 0.00000 | 0.025 | 1.000 | 3a | -3m |
| 4 | Mn | Mn1 | 0.00000 | 0.00000 | 0.50000 | 0.333 | 1.000 | 3b | -3m |
| 5 | Ni | Ni1 | 0.00000 | 0.00000 | 0.50000 | 0.309 | 1.000 | 3b | -3m |
| 6 | Li | Li2 | 0.00000 | 0.00000 | 0.50000 | 0.025 | 1.000 | 3b | -3m |
| 7 | Li | Li1 | 0.00000 | 0.00000 | 0.00000 | 0.975 | 1.000 | 3a | -3m |

Table-3: Profile Factor ($R_p$), Bragg Factor ($R_B$), Crystallographic Factor ($R_F$), Goodness Fit Factor ($\chi^2$), lattice Constant (*a*) and Unit Cell Volume of $LiNiO_2$ and $LiNi_{1/3}Co_{1/3}Mn_{1/3}O_2$

| Compound | $R_p$ % | $R_B$ % | $R_F$ % | $\chi^2$ | *a* (Å) | *b* (Å) | *c (Å)* | V $(Å)^3$ |
|---|---|---|---|---|---|---|---|---|
| $LiNiO_2$ | 21.3 | 5.859 | 7.016 | 20.3 | 2.8966 | 2.8966 | 14.2373 | 103.455 |
| $LiNi_{1/3}Co_{1/3}Mn_{1/3}O_2$ | 27.5 | 4.023 | 2.635 | 0.98 | 2.8577 | 2.8577 | 14.2269 | 116.1832 |

**Rietveld Refinement**

To examine the exact crystal symmetry of $LiNiO_2$ and $LiNi_{1/3}Co_{1/3}Mn_{1/3}O_2$, the Rietveld refinement was carried out using the preliminary XRD results. The refined diffraction patterns and fitting results are presented in Figures 3(a), 3(b), and 3(c). All Bragg peaks were modelled with the Pseudo-Voigt function.[12-14] A goodness of fit was obtained for both samples with the rhombohedral symmetry of the space group $R\bar{3}m$ . The crystallographic unit cell for $LiNiO_2$, which consists of rhombohedral symmetry, was depicted exclusively in Fig.-3(a). Compared to $LiNiO_2$, in the structure of $LiNi_{1/3}Co_{1/3}Mn_{1/3}O_2$, the lithium atoms occupy the 3a sites, the transition metal atoms (Ni, Co and Mn) occupy the 3b sites, and the oxygen atoms occupy the 6c sites. Furthermore, the refined lattice parameters, atomic positions, occupancies, and fitting parameters were represented in Table-1 to 3 for $LiNiO_2$ and $LiNi_{1/3}Co_{1/3}Mn_{1/3}O_2$,

respectively. The dominant diffraction peak at 2θ = 18.67° corresponds to the (003) reflection, with additional reflections assignable to the (104), (101), (107), (110), and (113) planes appearing at 2θ = 44.14°, 37.95°, 58.38°, 64.12°, and 67.48°, respectively. This diffraction pattern is characteristic of the hexagonal layered phase.[9] The resolution of the (018) and (110) doublet confirms a high degree of crystalline order. The patterns are well fitted, with the $R_{Bragg}$ of 5.859% and 4.023%, the $R_{wp}$ of 7.016% and 2.635% and one $Ni^{2+}$content in the 3a sites of 0.308 and 0.309, respectively. $Co^{3+}$ (0.63 Å) have a smaller ionic radius than $Ni^{2+}$ (0.69 Å). Thus, the lattice parameters for the $LiNi_{1/3}Co_{1/3}Mn_{1/3}O_2$ sample ($a$=2.8577 Å, $c$=14.2269 Å) are smaller than that of $LiNiO_2$ ($a$=2.8966Å, $c$=14.2373Å).

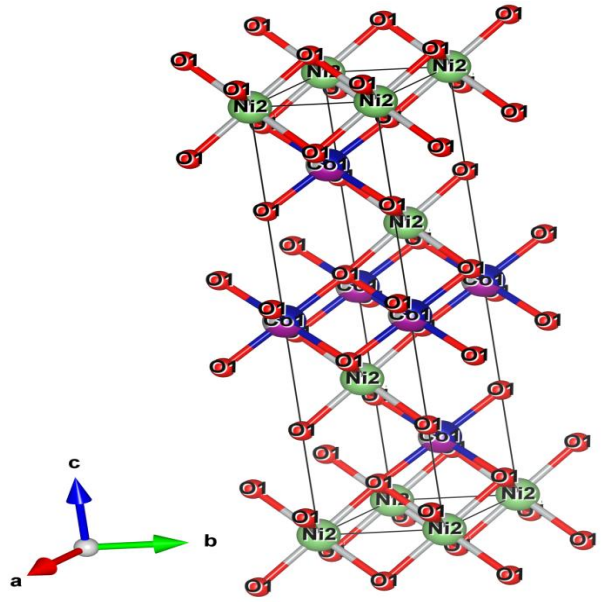


Fig.-3(a): Crystal structure of $LiNi_{1/3}Co_{1/3}Mn_{1/3}O_2$

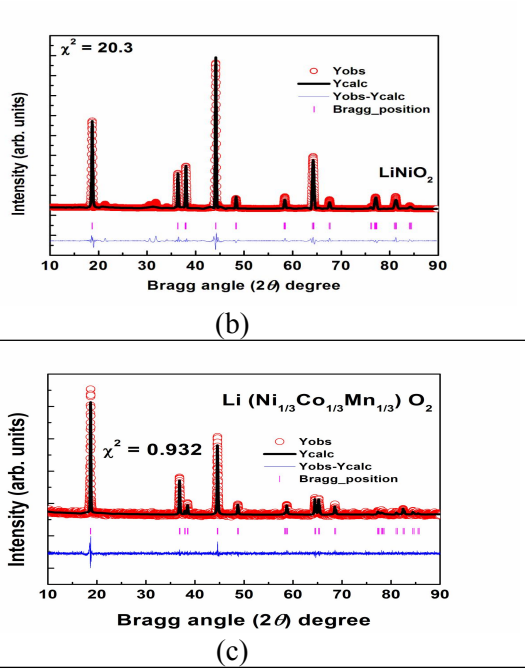


Fig.-3(b and c): Retveld Refinement of $LiNiO_2$ and $LiNi_{1/3}Co_{1/3}Mn_{1/3}O_2$

## Charge/Discharge Studies

Figure-4 (a) and (b) present the charge/discharge behaviour of the synthesized doped lithium cathode materials performed using a rechargeable CR2032 coin cell in the voltage range 3.0-4.5 V under a constant current density of 0·1 mA/cm$^2$. This section also performs and established comparative research on the electrochemical characteristics of $LiNiO_2$ and $LiNi_{1/3}Co_{1/3}Mn_{1/3}O_2$ compounds. Figures-4(a) and (b) depict the initial charge/discharge curves of electrochemical cells made of $LiNiO_2$ and $LiNi_{1/3}Co_{1/3}Mn_{1/3}O_2$, respectively, at a constant current rate of C/10 between 3.0 and 4.5 V. Quantitative capacity data for the first cycle at ambient temperature are tabulated in Table-4. During the initial cycles, two distinct voltage plateaus are discernible in both the charge and discharge profiles.

Table-4: Charge/Discharge Values of LN and LNCM Cathode Materials

| Compound | Charge (mAh/g) | Discharge (mAh/g) | Charge (mAh/g) (present work) | Discharge (mAh/g) (present work) |
|---|---|---|---|---|
| $LiNiO_2$ | 165.0 | 208.3 [5] | 160.19 | 103.75 |
| $LiNi_{1/3}Co_{1/3}Mn_{1/3}O_2$ | 197.0 | 172.0 [6] | 125.09 | 80.0 |

On the charge side, the plateaus appear near 4.45 V and 4.3 V, while the corresponding discharge plateaus are located at approximately 4.2 V and 4.3 V. The presence of these dual-plateau features reflects a two-stage mechanism for lithium-ion intercalation and deintercalation. An increase in lithium concentration progressively flattens the charge/discharge profiles.[15–17] $LiNiO_2$ is discovered to have a first discharge capacity of 252.0 mAh g$^{-1}$, while $LiNi_{1/3}Co_{1/3}Mn_{1/3}O_2$ has a first discharge capacity of up to 165 mAh g$^{-1}$ and an irreversible capacity of just 70 mAh g$^{-1}$. When compared to the $LiNiO_2$ cathode material, the

$LiNi_{1/3}Co_{1/3}Mn_{1/3}O_2$ cathode material showed about 98% discharge capacity retention at the conclusion of the 20th cycle.

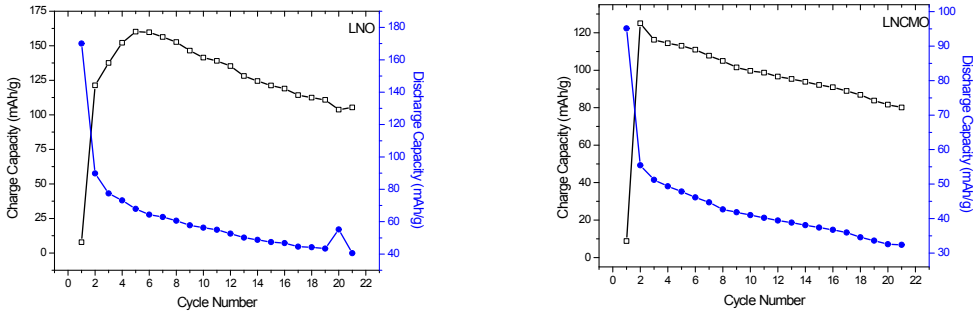


(a) (b)

Fig.-4: Charge Discharge Curves of $LiNiO_2$ and $LiNi_{1/3}Co_{1/3}Mn_{1/3}O_2$

## CONCLUSION

The X-ray diffraction, FTIR, and electrochemical values of $LiNiO_2$ and $LiNi_{1/3}Co_{1/3}Mn_{1/3}O_2$ cathode materials are thoroughly compared in this work. The $LiNi_{1/3}Co_{1/3}Mn_{1/3}O_2$ cathode material improves crystal stability and reduces $Li^+/Ni^{2+}$ disorder in the lattice, both of which are beneficial for Li+ ion and electron diffusion. All measured parameters show good correspondence with data available in the published literature. Rietveld refinement confirms the Rhombohedral structure with $R\bar{3}m$ space group for both the samples. The patterns are well fitted, with the $R_{Bragg}$ of 5.859% and 4.023%, the $R_{wp}$ of 7.016% and 2.635% and one $Ni^{2+}$content in the 3a sites of 0.308 and 0.309, respectively. Although a moderate reduction in initial specific capacity was noted, this was more than offset by substantially enhanced capacity retention during repeated cycling. These findings strengthen the both samples are optimistic for real-world uses is $LiNi_{1/3}Co_{1/3}Mn_{1/3}O_2$, particularly for high-rate lithium-ion batteries used in electric vehicles.

## ACKNOWLEDGEMENTS

The authors are grateful to Advanced Analytical Laboratory, DST-PURSE, Andhra University, Visakhapatnam, for allowing the use of facilities for this work.

## CONFLICT OF INTEREST

The authors declare that there is no conflict of interest.

## AUTHOR CONTRIBUTIONS

The present work is related to *SDG-7: Affordable and Clean Energy*. All the authors contributed significantly to this manuscript, participated in reviewing/editing and approved the final draft for publication. The research profile of the authors can be verified from their ORCID ids, given below:

K. Vijaya Babu https://orcid.org/0000-0002-6477-2910
K. S. K. R. Chandra Sekhar https://orcid.org/0000-0003-3608-1327
Ch. Srinivas https://orcid.org/0000-0001-8116-0337
Y. N. Rao and P. Ramakrishna: This is their first publication, and they do not have ORCID iDs.


**Cite this article as:** K. V. Babu *et al.*, *Rasayan J. Chem.*, 19(3), 1489-1494(2026), https://doi.org/10.31788/RJC.2026.1939588

## REFERENCES

1. T. T. B.Tran, E-J Park, H-I. Kim, S-H. Lee, H-J. Jang and J-T. Son, *Materials Letters*, **316**, 131810(2022), https://doi.org/10.1016/j.matlet.2022.131810

2. M. A. M. Cruz, G. R. Sanchez, M. O. Tolentino, H, Piffer and I. Gonzalez, *Journal of Alloys and Compounds*, **923**, 166328(2022), https://doi.org/10.1016/j.jallcom.2022.166328
3. Y. Kim, W.M Seong and A. Manthiram, *Energy Storage Materials*, **34**, 250(2021), https://doi.org/10.1016/j.ensm.2020.09.020
4. J. Chen, N. Zhao, G-D. Li, F-F. Guo, J. Zhao, Y. Zhao, T. Jia, F. Fu and J. Li, *Materials Research Bulletin*, **73**, 192(2016), https://doi.org/10.1016/j.materresbull.2015.09.031
5. C. C. Chang, J. Y. Kim and P.N. Kumta, *Journal of the Electrochemical Society*, **149**, A331(2002), https://doi.org/10.1149/1.1447136
6. Z. Hu, L. Wang, Y. Luo, Q. Wei, M. Yan, L. Zhou and L. Mai, *Science Advances Today*, **1**, 25218(2015).
7. J. M. Sailaja, K. V. Babu, N. Murali and V. Veeraiah, *Journal of Advanced Research*, **8**, 169(2017), https://doi.org/10.1016/j.jare.2016.11.003
8. C. Julien, C. Letranchant, S. Rangan, M. Lemal, S. Ziolkiewicz, S. Castro Garcia, L. El Farh and M. Benkaddour, *Materials Science and Engineering B*, **76**, 145(2000), https://doi.org/10.1016/S0921-5107(00)00437-8
9. L. Song, Z. Tang, Y. Chen, Z. Xiao, L. Li, H. Zheng, B. Li and Z. Liu, *Ceramics International*, **42**, 8537(2016), https://doi.org/10.1016/j.ceramint.2016.02.020
10. J. Valikangas, P. Laine, M. Hietaniemi, T. Hu, P. Tynjala and U. Lassi, *Applied Sciences*, **10**, 8988(2020), https://doi.org/10.3390/app10248988
11. R. Sathiyamoorthi, P. Manisankar, P. Shakkthivel, M. S. Lee and T. Vasudevan, *Bulletin of Materials Science*, **31**, 441(2008), https://doi.org/10.1007/s12034-008-0071-2
12. H. Li, Y. Zhang, X. Wang and J. Chen, *Electrochimica Acta*, **465**, 143002(2024), https://doi.org/10.1016/j.electacta.2023.143002
13. S. Kim, D. Lee and J. Cho, *Journal of Power Sources*, **602**, 234567(2024), https://doi.org/10.1016/j.jpowsour.2024.234567
14. Y. Wang, H. Sun, Z. Liu and L. Chen, *Ceramics International*, **50**, 11842(2024), https://doi.org/10.1016/j.ceramint.2024.01.112
15. X. Zhao, Q. Wang, M. Gu and Y. Yang, *ACS Applied Energy Materials*, **7**, 5561(2024), https://doi.org/10.1021/acsaem.4c00561
16. H. Park, J. Lee and K. Kang, *Journal of Energy Chemistry*, **82**, 415(2024), https://doi.org/10.1016/j.jechem.2023.11.018
17. R. Zhang, Y. Liu, F. Wu and L. Li, *Solid State Ionics*, **402**, 116245(2025), https://doi.org/10.1016/j.ssi.2024.116245

[RJC-9588/2026]